EUROPEAN JOURNAL OF BIOMEDICAL AND PHARMACEUTICAL SCIENCES
http://www.ejbps.com

ISSN 2349-8870
Volume: 11
Issue: 11
Year: 2024

SYNTHESIS, CHARACTERIZATION, AND ENVIRONMENTAL APPLICATION OF WO_3 NANOPARTICLES

Dr. Surekha Kannaujia*[1], Dr. Radhey Shyam[2], Dr. Sonu Dwivedi[3], Dr. S.V Tyagi[4] and Himanshu Bhatt[5]

[1,2,3]Associate Professor Chemistry, D.B.S. (PG) College Dehradun, 248001, (UK), India.
[4]Associate Professor Chemistry, D.A.V. (PG) College Dehradun, 248001, (UK), India.
[5]Research scholar Chemistry, D.B.S. (PG) College Dehradun, 248001, (UK), India.

***Corresponding Author: Dr. Surekha Kannaujia**
Associate Professor Chemistry, D.B.S. (PG) College Dehradun, 248001, (UK), India.

Article Received on 19/09/2024 **Article Revised on 09/10/2024** **Article Accepted on 29/10/2024**

ABSTRACT
Tungsten trioxide (WO_3) nanoparticles were synthesized by a citric acid monohydrate and gelatin-assisted precipitation method using a ratio of Sodium tungstate (Na_2WO_4), citric acid monohydrate ($C_6H_8O_7.H_2O$) and gelatin powder ($C_{102}H_{151}N_{31}O_{39}$). The formation of the monoclinic crystal structure of WO_3 at different temperatures was confirmed by X-ray powder diffraction (XRD). The characterization of the synthesized samples was complemented by scanning electron microscopy (SEM), Fourier Transform Infrared Spectroscopy (FTIR), Energy-dispersive X-rays (EDX), etc. The nanoparticles generated were found to have rectangular and oval morphologies. The photocatalytic ability of WO_3 nanomaterials to destroy RhB dye in aqueous solutions at various pH levels was investigated. The results show that at pH 8, WO_3 nanomaterials have the best photocatalytic activity. Irradiation with a lamp for 80hours resulted in the maximum mineralization of 98%.

KEYWORDS: Tungsten trioxide nanoparticles, citric acid, gelatin powder, X-ray powder diffraction, SEM, FTIR, Photocatalytic ability and pH levels.

1. INTRODUCTION

1.1 General

There still are substantial proportions of organic compounds pollutants in wastewater in the textile industry, which has serious impacts on the environment and human life [Kiwaan et al., 2020]. Various forms of environmental contamination, notably air and water pollution, are wreaking havoc on the ecosystem across the world. Organic dyes are found in high concentrations in waste effluents from the papers, fabric, and polymer industries [Karthikeyan et al., 2020]. The greywater from major textile countries is discharged into water bodies, which eventually flow in to the sea. In India, taking an example of city Kanpur which is a major textile hub that dumps massive quantities of sewage-water into drains and streams, subsequently draining into the Bay of Bengal and River Ganga [Kishor et al., 2021].

Textile dyes and other industrial dyestuff are one of the most common organic chemicals that pose a conspicuous threat to the preserve around 120% of global world dye production is destroyed and emitted in textile effluents the escape of these colored waste flows into the habitat is an essential example of nano pollution, eutrophication, oxidation hydrolysis and other chemical phenomena that occur in the wastewater phase can cause dangerous byproduct [Konstantinou et al., 2004]. The various their great robustness to climate, illumination, water, detergents, chemicals, and other characteristics, for example, bleach as well as sweat, many of these dyes' exodus from routine sewage-water treatment techniques or stay in the surrounding [Chequer et al., 2013]. Even though most corporations 81 utilize dye and their industrial domestic sewage incorporates 82 huge volumes of dye, these dyes are 80 considerable polluters. Although they feature composite 84 molecular structures that make them more stable toward 85 light and impervious to biodegradation, several dyes are nonbiodegradable in water [Natarajan et al., 2017]. Dye-containing sludge should not have been discharged into bodies of water. Dyes cause direct toxicity to bacterial communities by suppressing growth, hindering light penetration, slowing photosynthesis rate, and inducing respiratory depression in aquatic ecosystems. [Hassani et al., 2013].

1.2 Dyes Industrial and Process

Dye business sewage treatment techniques are a distinctive important characteristic in dye manufacturer trade that is unsuccessful. Fibers are produced by the dye

companies, which are then spun into yarn and finally processed into textile products. Textile finishing procedures are used to generate these commodities. The unsettled dye is rinsed off with water during the textile dyeing process. When opposed to the wet technique, the dry technique generates a lot of solid waste. [Shindhal et al., 2021]. Numerous methodologies have been offered to cure the water poisons that all vertebrates in our biosphere are dealt with in the past decades, spanning major ecological concerns. [Saravanan et al., 2015]. Beneath alkaline circumstances, reactive dyes create covalent interactions with hydroxyl groups of rayon, typically by nucleophilic attack or addition. Superior wash fatness features would be predicted as a function of these deep ties. The dyes, on the other hand, can react using hydroxyl groups with water, rendering them incapable of reacting with cellulose. As an outcome, low reactive dye fixing and excessive sugar concentration would generate global pollution [Ahmed et al., 2005] (Fig.1).

Dyes are made of various materials being used in a wide range of sectors, including fabrics, beauty products, papers, leatherette, pharmacology, and food. Upwards of 100,000 are commercial - available. Dyes are available, with an expected annual production of more than 7105 tones, 15% of which is squandered during the synthetic dyes [Hai et al., 2007]. According to the World Bank, aquifer depletion in the textile and apparel industry is triggered by printing and dyeing treatments that are administered to the garment. The wastewater emitted by the dye wastewater industries involved a total of 72 toxic materials, 30 of which are insoluble in waste treatment methods. [Bhatia et al., 2017]

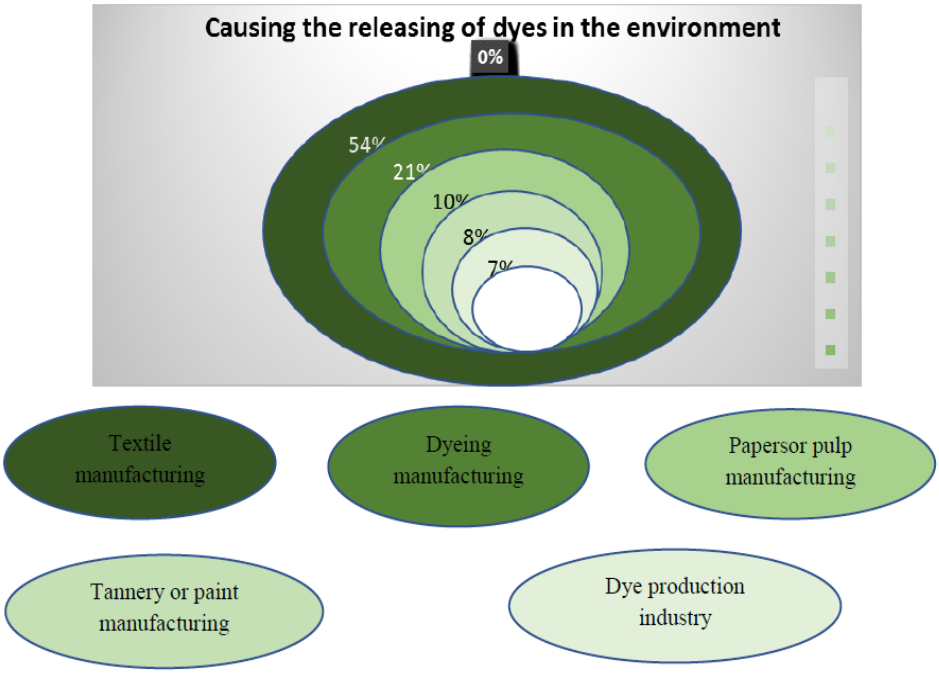

Figure 1: Organizations that discharge dyes into the wastewater stream in large quantities.

1.3 Methods used in dye wastewater treatment

The vast majority of dyes are not degradable in ordinary sewerage systems due to their high stability under daylight and immunity to microbial assault and temperature. Over the last two decades, there has been a growing recognition of the importance of effective and appropriate technologies to decolorize and degrade dyeing industrial effluents in order to reduce their ecological footprint. The primary approaches for removing these contaminants are visualized in Figure 2. [Martınez-Huitle et al., 2009]. Considering common approaches for decolorizing synthetic dyes in wastewater are unsatisfactory, adsorption of textile chemicals on economical and convenient solid supports has been recommended as a straightforward and cost-effective method alternative to their eviction from water and sewage water. The adsorption parameters of a large variety of physicochemical and biological supports have been determined, as well as their removing synthetic dyes [Forgacs et al., 2004]. The most broadly utilized methods of dye removal from decolorization industrial events are systematically analyzed in this section. Three categories of methodologies have been discussed: Biological, chemical, and physical [Robinson et al., 2001].

One of the most promising advanced oxidation mechanisms for the destruction of water-soluble emerging pollutants dissolved inorganic and wastewater is heterogeneous photocatalysis using a blend of TiO_2 and UV light. When TiO_2 particles are illuminated by light with a frequency of 390 nm, one electron is excited out of its energy level, leaving a hole in the valence band. To generate Electrons are promoted from the conductive band via electron-hole couples of TiO_2 [Khataee, et, al., 2009]. The cost of electrode material

and used electrical energy in comparison to the value of chemicals, as well as the demand for easy separation phases, are the most important elements that determine the electrochemical process' operational expenses. As a result, these two aspects were found significant price variables linked to specific. Once hazardous residual amounts of impurities are found in the ending foamy effluent or particles in the material generated, chemical treatment can exacerbate toxicity. Final therapeutic approaches become less likely to occur. To eliminate residual amounts, hence chemicals deployed in the advanced parts of sewage water cure of special concern. Therapeutic additives like coagulants and flocculent aids, when taken as prescribed, can also help with toxicity treatment [Mutairi et, al., 2006]. The major step in the coagulation-flocculation process is to incorporate reagents to destabilize pollutants from water that are dissolved or suspended the collapsing contaminants are then agglomerated creating folcs, which could perhaps be calmed or taken out of the water and sewage-water via subsidence [Mahmudabadi et al., 2018].

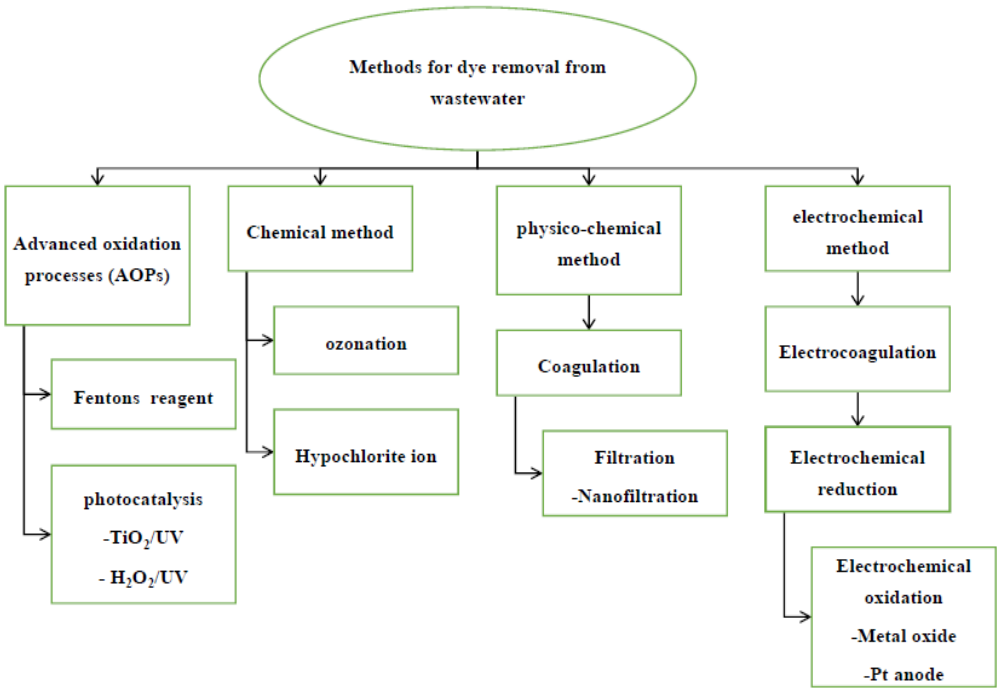

Figure 2: Different methods used in dye wastewater treatment.

1.4 Advanced oxidation process

Advanced oxidation processes (AOPs) have suddenly gained significant attention as a revolutionary wastewater treatment method. In AOPs, the non-selective degradation of a broad array of toxic compounds is enhanced by the hydroxyl radical (OH•), which is released owing to the increased oxidation potential [Rahmani et, al., 2019]. Toxicity symptoms of water have become a serious threat to the environment as a result of fast rapid industrialization. Due to its carcinogenicity and mutagenicity, hexavalent chromium is an ion of trace metals originating mostly from the industries operations metal working, metal plating, tannery, and dyeing and textile are just a few examples and is extremely harmful to living organisms [Li et. al., 2020].

The synthesis of oxide hybrids has been shown to be a beneficial approach to increasing the photovoltaic activities of titanium dioxide materials. The physicochemical and optical attributes of the hybrid are governed by the modifier adopted and its compatibility with the substance. Each of the modifiers has a huge impact on the material's surface charge, enhancing or weakening its photocatalytic potential [Siwinska-Stefanskaet, al., 2018]. Reaction frequency, Hydrogen peroxide/Iron (II), pH, TiO_2 content, ozone concentration, and UV intensity are all factors to consider all impact the advanced oxidation treatment of municipal wastewater. As a result, to save both money and effort, it is required to discover the appropriate number of parameters by running the fewest number of experiments. The implementation of Response Surface Methodology is a practical way of optimizing parameters and assessing their interactions [Hassanshahi et. al., 2018].

The applicability of AOP to waste sewage treatment must reflect that it utilizes expensive reactants such as H_2O_2 and/or O_3 shown in figure 3, hence it is essential that it should not be used in place of more premium treatments which include biological degradation [Andreozzi et al., 1999]. Fenton presented the first investigation on the breakdown of organic molecules by a mechanism that is not identified at the time as happening through hydroxyl radical reactions. In the

presence of trace quantities of ferrous (Fe^{2+}) salts and hydrogen peroxide, tartaric and racemic acids are destroyed in solutions, however, Fenton did not study the mechanism of this reaction. Fe^{2+} lowers H_2O_2 by the generation of hydroxyl radicals, thus according to Haber and Weiss (1932). AOPs are based on the in-situ synthesis of •OH radicals by chemical, photochemical, coagulation-flocculation, or electrochemical phenomena. The Fenton methodology, which contains a blend of a soluble, a non-soluble iron (II) powder and H_2O_2, known as the Fenton's reagent, to degrade and eliminate POPs, is the largest and most commonly used chemical AOP [Oturan et al., 2014].

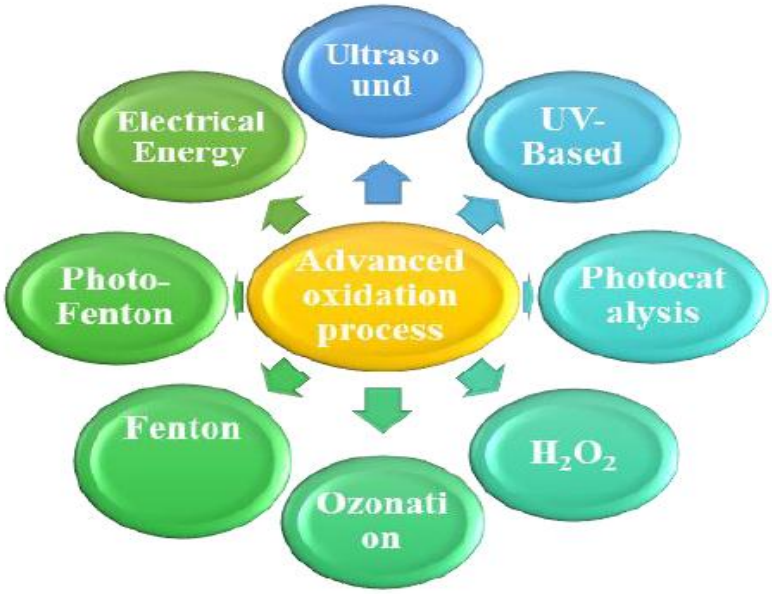

Figure 3: Different AOP techniques used in dye wastewater treatment.

1.4.1 Photocatalysis

The outcome of certain examinations will be affected by the choice of an appropriate photocatalyst. Normally, catalysts are chosen based on a variety of factors, including the productivity of the catalysts potential to eliminate a contaminant, the material's stability, energy gap, and so on. Another of the main contributors to high efficiency in dye photocatalytic degradation is the band gap of the type of semiconductor [Nazri et al., 2020]. The word "photocatalysis" is still a point of contention. It is maintained, for instance, that the concept of a photocatalyzed synthesis is fundamentally erroneous since it suggests that light serves as catalysts in the synthesis, but light always functions as a mediator that is absorbed in the reaction mechanism. In truth, the phrase "photocatalysis" is widely used that's here to stay; it does not entail catalysis by illumination, and should never be used to do so; rather, it refers to the "momentum of a photoreaction by the presence of a catalyst." To a certain effect, the word "photoreaction" is often referred to as a "photoinduced" or a "photoactivated" reaction. The phenomenon of "photosensitization" is included in the above definition of "photocatalysis [Mills et al., 1997]. Sunlight causes most of the spontaneous cleansing of aquatic ecosystems lagoons, lakes, streams, riverfronts, and glaciers by breaking down large molecules into smaller molecules and eventually carbon dioxide or other industrial minerals. Various natural pretreatments help to speed up the process. In 1976, 'colloidal semiconductors' was discovered, as well as the use of catalysts to stimulate certain redox mechanisms on understanding the types [Beydoun et al., 1999].

The essential criterion for an effective photoactive layer is that the electron couple's threshold voltage, e^-/h^+, be contained within the photocatalyst's energy gap zone. The energy content at the bottom of the conduction band determines photoelectrons' reducing potential, whereas the oxidizing potential is dictated by the calorific value at the top of photo-generated electrons is determined by the excited state at the valence band edge [Gupta & Tripathi 2011].

1. General scope

Clearwater is a valuable part of nature that is now under significant stress as a result of industrialized civilization's increasing usage. Because of the scarcity of groundwater, there is a growing demand for sewage disposal, recycling, and reuse for industrial uses. Physio-chemical biological, integrated treatment techniques and other technologies are among the various methods for removing contaminated chemicals from water. Surrounding restrictions become are now more significant in most phase of the fiber industries process across the global given the narrow execution regulatory issues, it is impossible to adopt eco-friendly fiber manufacturing models that eliminate each of the faults from the start to the finished product. The key problem is to come up with a design that is both cost-effective and uses less toxic or readily treatable chemicals as a

replacement. An acceptable system of treatment methods was designed based on garbage parameters and literature research.

1.1. Conventional treatment methods

Physiochemical properties treatment methods in the form of primary treatment, overall shape, and from before they are widely anticipated, according to many research organizations across the globe. The Enhanced Oxidation Process is a wastewater mechanism that is gaining popularity. It is a recommended method for removing organic debris. The creation of hydroxyl radicals (OH•) from hydrogen peroxide (H_2O_2), ozone, a series of pictures, or oxidizing agents, as well as the utilization of UV light, is the core premise of AOP. The OH• is principally responsible for the destruction of organic molecules. The Fenton reagent (H_2O_2 / Fe^{2+}) is one of the most efficient methods to oxidize organic pollutants among numerous. The Fenton chemical has been shown to be successful in the treatment of a wide range of industrial wastewater chemicals, including aromatic amines, a wide range of dyes, and a variety of other molecules, such as poisons and lubricants bugs [Mokif et al., 2019]

2. Photodegradation

Photocatalysis is a method for decomposing or degrading organic contaminants that is pure, long-lasting, and ecologically benign. Because they totally deconstruct harmful materials or transform them into – anti forms, photocatalysts treatment removes organic contaminants from polluted water without leaving harmful products behind. Photochemical remediate is a type of advanced oxidation that occurs in the presence of a photocatalyst. Photons with a power substantially greater than the band gap energy in between the photocatalyst's conduction band are absorbed by photocatalyst. Charge dispersion is caused by absorbing a photon, which enables to be excited from the band to the conduction band, accompanied by the production of positive electron holes. The chemical deconstruction of big molecules into smaller, not harmful, and low-molecular-weight species utilizing the broad spectrum of sunlight is known as photo-degradation (PD). It is a photocatalytic process that uses sunshine to successfully metabolize organic pollutants using considerably easier redox reactions [khan et al., 2020]

The goal of this study is to provide the present status in the field of polymer-based photocatalysts comprising the most common inorganic nanocrystals with strong catalytic activity underneath UV Visible light, such as TiO_2, ZnO, and CeO_2. [Melinte et al., 2019]. The degradation process provides a number of benefits over standard treatment technologies such chemical oxidation,18 adsorbents adsorption,19 biologically treatment,20 and so on. The phase transfer of contaminants without breakdown in the activated carbon adsorption process presents a new pollution challenge [kumar et al., 2017]

2.1. TiO_2 based semiconductor

Photocatalyst technology, which is both environmentally beneficial and cost-effective, has been widely used to combat pollution and waste scarcity. Since Fujishima and Honda first showed photocatalytic water splitting using a TiO_2 electrode under UV light in 1972, semiconductor photocatalyst technology has been widely applied in organics destruction, CO_2 reduction, thermal decomposition, and toxic metal ions minimization [Sun et al., 2022]. Alternative techniques were used to investigate the crystallographic, morphology, chemical, and photoluminescent characteristics of the produced nanomaterials. The produced TiO_2 quantum dots have a well-crystalline phase and strong photoluminescent characteristics, according to the comprehensive analyses. The photo-catalytic deterioration of an aqueous phase of Indigo carmine pigment under UV light irradiation was also used to examine the catalytic activity of produced quantum dots [Sood et al., 2015].

The geometrical, structural, optical, and photocatalytic capabilities of well-crystalline anatase TiO_2 nanoparticles were studied using a simple solution technique. The comprehensive investigations revealed that the as-synthesized nanostructures are well-crystalline, densely generated, and have good optical features. Paints, polymers, papers, ink, elastomer, textiles, cosmetics, leather, and ceramics all employ TiO_2 as a non-toxic white pigment. Pesticide degradation rate using TiO_2 and other catalysts has shown promise as a potential water clean-up approach. Titanium dioxide was also useful to clear the air in fruits, vegetables, and storage of cut flower spaces to cure rotting or extend the life expectancy products by breaking lower the ethylene gas generated in rooms of storage into CO_2 and H_2O. TiO_2 NPs show promise as an effective source of nutrients for seedlings, increasing biomass output and nutrient consumption via stimulating microbial activity [Deshmukh et al., 2018].

2.2. ZnO-based photocatalysts

ZnO as a photodiode, possesses the capacity to biodegrade every hazardous compound in the presence of UV rays due to its power of straight-line huge disparity, the charge density of sixty mega-eV, the droplets' capacity to stay put imaging and corrosion chemical, low hazardous, insoluble, photocatalyst ability, or the energy gap [Bagheri et al., 2019] compared to other iron oxides, zinc oxide (ZnO) is a viable choice as a solar light photocatalyst material because it has excellent photocatalytic energies for the destruction of organic contaminants [Danwittayakul et al., 2015]. The frequency of active sites rose as the mediator content increased as a result of a rise in the amount of zinc oxide material, but as a photo-activated activity, the photo-activated quantity of the solution dropped. At lower concentrations of solute, there is surplus balance across varying impacts is evenly balanced at binding sites, and the volume of Zinc oxide makes no difference from the equilibrium constant. The availability of extra active

sites exceeds the reducing photo-activated volume at high solute concentrations, resulting in a much higher k value as ZnO concentration is higher [Pare et al., 2008]. Yet, there are several issues with using ZnO powders, including (a) difficulties extracting the powder from the liquid after the reaction occurred, (b) particle aggregating in suspension, especially for large loadings, and (c) difficulties applying to continuously flow systems[Muthirulan et al., 2012].

2.3. CdS based photocatalysts

Numerous semiconductor photocatalysts, including as CdS, ZnS, CdSe, TiO_2, and others, have gotten a lot of attention for their ability to degrade organic dye pollutants in water. CdS is the most extensively utilized material among those whose Photocatalytic capabilities have been explored since it is effective, stable, safe, and affordable [Desai et al., 2017]. Cadmium sulfide (CdS) is the most basic and useful photocatalyst in environmental remediation and one of the most significant single crystals (bandgap 2.4 eV), which absorbs in the field of view. However, because to certain major flaws, such as particle aggregation, photo corrosion, and the short lifespan of light-generated components, the practical use of CdS in photocatalysis is limited. Various attempts have been done in this regard to increase CdS photocatalytic activity and stability, including morphology modifications, ion doping, and electronic hybridization, among others. It is well understood that the photocatalytic activities of nanostructured materials are strongly influenced by their individual features, such as size, bandgap, morphology, spatial topologies, and, in particular, porous structure. [Ullah et al., 2021]. Clean CdS and various concentrations of Sn-doped CdS nanoparticles were synthesized to remove MB contaminants from water. All of the samples were subjected to a photocatalysts examination in the sunshine [Venkatesh et al., 2020].

2.4. SnO_2 based photocatalysts

Along with its great chemical stability, nontoxicity, low cost and strong photoactivity, SnO_2 has been examined as an appealing and promising catalyst option. The morphology, electrical structure, crystal size, porosity, crystallinity, surface area, surface active sites, and surface defects of SnO_2 are all influenced by the process conditions and thread procedures. UV irradiation of SnO_2 produces extra electrons, which reduce and oxidize pollutants from aqueous on the surface, resulting in radical species such OH and O^{2-} radicals, which can break down most organic molecules [Sadeghzadeh- Attar et al., 2017]. Tin oxide (SnO_2), a well-known n-type semiconducting oxide, has been shown to have a large band gap of around 3.6–4.0 eV. Many investigations on creating SnO_2 nanostructures such as nanofibers, nanowires, nanorods, and nanoparticles were conducted so far. SnO_2 -NPs have been used of field of stable sensors, lithium-ion, optical and electronic devices, solar cells, energy conversion, oxidation catalysts, and photocatalysts pollution remediation due to their optical, electrical, electrochemical, and catalytic capabilities. Researchers have used a variety of physical and chemical methods to synthesize SnO_2-NPs throughout the years, spanning sol–gel, coagulation /flocculation, ultrasonic social decay, hydrothermal, convection, and chemical oxidation [Najjar et al., 2021]

Photocatalysis was employed to breakdown a wide variety of organic contaminants into harmless CO_2 and H_2O using various transition metal oxides such as TiO_2, ZnO, Bi_2O_3, Fe_2O_3, and SnO_2. SnO_2 has been discovered as a potential photocatalyst among them. SnO_2 has several advantages, including high electron mobility (100, 200 cm 2 V 1), high health and medical, non-toxicity, cheap cost, and processability, making it a possible choice for organic decolourization [Rani et al., 2020]

2.5. WO_3 based photocatalyst

The physical characteristics and photocatalysis efficacy of produced WO_3 salt was investigated in about W precursor type and pre-treatment settings. In the addition of separable additives, water photo oxidizes to oxygen and ions Cerium4+ was utilised mechanism to evaluate the powder activity under bright and near IR light [Bamwenda et al. 2001]**.** Tungsten oxide (WO_3), on the other hand, is a photocatalyst that responds to visible light and absorbs light up to 480 nm. WO_3 is cheaper to design, alter, and encapsulate surfaces with than mixed metal oxides and doped oxides. WO_3 is also pro and stable in acidic and oxidative circumstances [Sayama et al., 2010]**.** The water photo-electrolysis, tungsten trioxide semiconductor thin films that are porosity and nanocrystals were utilized as electrodes. Because Cells that split water commonly function in acid environments, the goal of this study is to see how tungsten trioxide electrodes with proton complexation affect the photo-electrolysis process performance. For this, a preliminary investigation of the capacity charges and discharges of protons electrodes were carried out under cathode and anode potentials, Although, at various voltages and periods. In a photoelectrochemical cell (PEC), Electrodes that had been protonated were used subjected to simulated solar light and characterised Chronoamperometry and straight sweep voltammetry were used in this study. In this study, the parameters for reversible protonation of tungsten trioxide nanostructured photo-anodes were investigated [Calero et al., 2013]

2.6. Brief discretion of Photocatalysis mechanism

Photocatalysis mechanism

Photocatalysis combines chemical kinetics and catalysis, requiring both light and a catalyst to complete a chemical reaction. Due to their unique electrical structure, semiconductors operate as a catalyst. The energy gap between the full valence band (VB) and the empty conduction band (CB) in semiconductor materials is termed the bandgap, and it is measured in electron volts. The semiconductor may be activated by a photon with

the same energy as the bandgap energy, An electron from the Valance band jumps to the CB, and vice versa. Since the leftover vacancy in the Valance band B, denoted as a hole (h1), and the electrons (e2) in the CB are both free to migrate through the crystal lattice, this is an important stage in a photocatalytic process. These free-charged particles are involved in the oxidation and reduction reactions that occur during the breakdown of organic contaminants. Furthermore, this liberated electrons or holes will sometimes recombination, generating heat as a byproduct. As a result, Photocatalyst is distinct from other types of water purification, procedures in that it concurrently performs both oxidation and reduction reactions. The reducing process is good for getting rid of dissolve hazardous ions, whereas the reaction of oxidation is good for getting rid of dissolved poisonous compounds that are organic. The wavelength of light shining on the catalyst surface affects the reaction photocatalysis can be performed by two distinct methods [Rajbongshi et al., 2020]

Although the precise process of photocatalysis is rather complicated, the underlying concept remains the same. When light with a strength more than or comparable to the bandgap of the semiconductor photocatalyst is irradiated, electrons are driven from the valence to the conduction band, huge holes in the conductive band. The existence of the hole is critical for the photocatalyst's destruction of the pollutant deposited on the catalyst's surface. Direct oxidation via reactivity with the surface-bound hydroxyl radical or indirect oxidizing by interaction with the flooring hydroxyl radical (•OH) (surface-trapped h+) or direct oxidation via h+ bonded to metallic surface, before it has been caught within the nanoparticle or at its interface [Zhang et al., 2018].

$TiO_2 + h_v \rightarrow e^- + h^+$

$h^+ + Mn^+_{ads} \rightarrow M_{ads}^{(n+1)+}$

Experimental

The materials and experimental procedures used for (EC) electrochemical, (STW) treatment of synthetic textile wastewater, containing basic colors, as well as the removal of dyes that are harmful to living organisms.

1. Materials

All the chemicals used in this study were of analytical grade. Sodium tungstate (Na_2WO_4), Sodium hydroxide (NaOH), Gelatin ($C_{102}H_{151}N_{31}O_{39}$), nitric acid ($HNO_3$), citric acid monohydrate ($C_6H_8O_7.H_2O$).

2. Dyes wastewater

The study of dyes effluents containing a rhodamine b dye are used for the solution. The rhodamine b solution was prepared for synthetically as per method for they are reported in the literature using chemicals. These effluents are commonly found in various types of industries. [Ritika et al., 2018]. Mainly are used for the textile industries. For the research degradation mechanism rhodamine b dye. A stock solution was prepared 1000 mg/l of the solution was prepared. The stock solution was diluted using distilled water for getting required concentration of dye solution.

Table 1: Characterization of the rhodamine B dye.

Colour index name	C.I. basic violet 10
Colour index number	45170
CAS number	81-88-9
Chemical class	Amphoteric in nature
Chromophore	melatonin
Common name	Rhodamine b
pH vale	7.40-4.00
Molecular formula	$C_{28}H_{13}ClN_2O_3$
Molecular weight	479.01
λ_{max} (nm)	553

3. Experimental methodology

3.1. Preparation of WO_3

To prepare sodium tungstate, 0.05mol of Na_2WO_4 was added to 25ml of deoxygenated water (for 30min. continuous stirring), then 0.054mol of $FeSO_4.7H_2O$ and 0.027mol $FeCl_3.6H_2O$ were successively added dropwise into 9ml of 1mol NaOH solution under vigorous mechanical stirring at 50^0 C which formed the black precipitate. After continuous stirring for 60 min, the precipitate was separated and the supernatant was removed by decantation. Now, distilled water was added to the precipitate and the solution was discarded after centrifuging at 5000 rpm. Repeated the same procedure three times and then precipitate it with ethanol twice, after drying at 70℃ in a vacuum for overnight black nanoparticles were obtained. A portion of the black nanomaterials was calcined in air for 1 hour at 5000℃. It was essential to receive red-brown particles.

3.2. Preparation of WO_3 with citric acid

WO_3 nanomaterial was synthesized by the precipitation method in the presence of citric acid. For this purpose, 0.0017moles of sodium tungstate (Na_2WO_4) were added to 50ml of nitric acid (HNO_3) by continuous stirring at 70^0C. Then 0.00269moles of citric acid monohydrate were added to the solution under continuous stirring and maintained at a constant temperature until the formation of a yellow-green solid precipitate. Took it into the centrifuge tube and centrifuge at 5000rpm, discarded the unwanted solution, and collected shown in figure 1. This

material was used as a precursor for the WO_3 nanomaterials, the precursor obtained was decomposed by the thermal treatment at 500^0C for 4 hours. This sample will be identified hereafter as WO 500 respectively.

Figure 1: Prepared WO_3 with citric acid.

3.3. Preparation of WO_3 with Gelatin

Synthesized WO_3 nanomaterial in presence of Gelatin Powder. A total of 0.017mol of sodium tungstate (Na_2WO_3), were dissolved by a magnetic stirrer at 70^0C in 50mL of nitric acid solution (5% v/v HNO_3). Then 0.026 mol of gelatin Powder ($C_{103}H_{151}N_{31}O_{39}$) was added to the solution under continuous stirring and maintained a constant temperature until the formation of yellow-green precipitate was carried out. Centrifuge the solution at 5000 rpm and the undesired waste solution was discarded and then collected into the porcelain capsule. The formation of WO_3 was decomposed by the thermal treatment at 500^0C for 3.5 hours. This sample is denoted as WO-G.

Figure 2: Treatment of dye degradation.

3.4. Fourier transformation infra- red spectroscopy (FTIR)

The use (FTIR) spectrophotometer (Thermo-scientific instruments corporation, united states of America) we find the functional group present in the manufactured particle. The working of the FTIR is lower as compared to UV region. The range of FTIR is may be classified in three regions, near infra-red region the range is (12500-4000 cm^{-1}) this region is overtone, second is middle infra-red region (4000 to 200 cm^{-1}) this region is known as vibrational region and third is far infra-red region between (200 to 10 cm^{-1}) this region is rotation region.

The working range of FTIR is 667 to 4000 cm-1. A region among 1300 to 4000 cm^{-1} determines the functional group. So, this region is called as functional group region. Region between (667 to 1300 cm^{-1}) this region is known as finger print region and these two identical compounds have exactly same spectra when run in the same medium under similar condition. The principle of infra-red spectroscopy (FTIR) is based on the absorption of IR radiation causes an excitation of molecules from a lower to higher vibrational level. So, this spectroscopy is known as vibrational spectroscopy. The electromagnetic radiation interacts with the sample, the absorption of Infra-red radiation by molecules there is a transition between vibrational energy level. Molecule is gone from lower to higher vibrational energy level. All the molecule bond present but do not absorb infra-red radiation. Infrared radiation can be absorbed by bonds that have a shift in dipole movement. This type of vibration is called infra-red active vibration. There are two types of vibration present one is stretching and bending vibration.

3.5. Scanning electron microscope (SEM) and energy-dispersive x-ray analysis (EDX)

Scanning electron microscope (SEM) is method we focus on a beam of electrons is used for the scanning of the sample and image of the sample is produced. In this process electron interact with sample atoms produce many types of signals. These signals contain the information about sample surface morphology, ideography and composition. In the SEM technique electron beam is used instead of light to produce image. When an electron beam of light interacts with sample another electron such as back scattered of light or secondary beam of electron are affected. A secondary beam of light and scattered electrons is collected by the detectors are converted into a signal. A collecting signals image and sample produced on the surface. This method is mainly used for the identification of sample by this microscopy morphology of the particle should be determined. Energy dispersive x- ray spectroscopy (EDX) is a most important technique. They provide the information about the elemental composition of the sample surface and back scattered x rays and it is providing the information for mapping of the elemental features fast differentiation in multiphase materials and the surface of the materials. An elemental analysis for the required solid sample at different locations analysis with the EDX accessory. Their materials were the first ground to make them homogenous, and then distributed out on the sample was placed to create flat surfaces.

3.6. X-ray diffraction (XRD)

X- ray diffraction (Regaku) is an analytical technique are used in material science to determine the crystallographic structure of the material. The range of XRD is work between 0.01nm - 10 nm. X- ray diffraction technique works by irradiating a material with incident x rays and then measuring the intensities and scattering angles of the x rays and that leave the material. The XRD is used for mainly the sample which have crystalline nature and do not for amorphous. In the crystal means position of atoms are arranged in is determined from the electron density and measured type of bond and chemical bond length.

3.7. Photo catalytic degradation of dye

The degradation of rhodamine b dye is observed under the ultra violet light irradiation with the respect to time. Prepare WO_3 catalysts are used in the photocatalytic reduction of the dyes present in the waste water. The dyes are very harmful to humans, animals, and nature. The dyes effluents are discharged from various industries such as textile industries, leather industries etc. There are present various types of impurities in dye effluents. We used synthesized photocatalyst in the degradation of rhodamine b dye. To analyse the photocatalytic activity of the photocatalysts. Firstly, we take the 10 mg L^{-1} of rhodamine b dye add into 1.0 L distilled water then added 1.5 g L^{-1} of WO_3 into solution. The solution of rhodamine b after adds into photocatalysts and 1.0 M hydrogen peroxide solution in a beaker. The solution was put in the magnetic stirrer in a closed chamber in the presence of UV irradiation light (bulb 250 w). The RPM was maintained about 500 to 600 and no need for extra temperature. The sample was collected at 30, 60, 90, 120, 150, 180, minutes time intervals. The intensity of the solution and colour was measured by the UV -visible spectrophotometer. The range of UV visible spectrophotometer is 200 to 800 nm. The maximum absorbance of rhodamine b dye is 546 nm, check for the UV visible spectrophotometer. Rhodamine b dye is an amphoteric nature. It is show both of character acidic and basic.

4. RESULTS AND DISCUSSION

The results and discussion concerning to photocatalysis of organic pollutant containing wastewater from aqueous solution using WO_3.

1. Characterization of materials

XRD measurements have been used to analyze the crystallinity of the mesosphere semiconductors. The XRD of the WO_3 is illustrated in Fig.1. For WO_3, the sequence of sharp and strong diffraction peaks was consisting of WO_3 along with about O_2 deficient WO_3, and the corresponding (hkl) values of different peaks were indexed to comparison with the standard JCPDS data files (Monoclinic-WO_3). (Fig.1) has been presented with the highest peak intense at ~ 32.55° corresponding to (hkl) value (120) for pure WO_3 monoclinic. The occurrence of new peaks in considerable proportions perfectly matches with oxygen-deficient WO_3 [Singh et al., 2014] The perfect peaks at 76.52° (222), 68.49° (220), 57.78° (202), 41.15° (022), 34.98° (120), 33.25° (200), 38.55° (020), 24.90° (022), corresponding to tetragonal and hexagonal, respectively. Higher O_2 deficient phases in the WO_3 sample recommend n-type carrier concentrations and excellent photocatalytic performance of as-prepared semiconductors. As shown in Fig. 1, the

multiple diffraction data including multiple diffraction peaks at 2θ and their corresponding crystallographic planes of 24.90° (022), 38.55° (020), 33.25° (200), 34.98° (120), 41.15° (022), 57.78° (202), 68.49° (220), 76.52° (222) match well with WO_3 orthorhombic crystal structure (JCPDS card no. 79-2381), and no other impurities peaks were observed showing the higher phase purity of as-prepared samples with crystallite size of 8.32 nm.

The XRD pattern of calcined WO_3 the sequence of sharp and each strong Bragg diffraction peaks confirm the polycrystalline nature of the as-prepared material. The WO_3 sample illustrates the diffraction peaks planes (002), (020), (200), (120), (022), (202), (220), and (222) correspondingly to the diffraction angle peaks 76.52°, 68.49°, 57.78°, 41.15°, 34.98°, 33.25°, 38.55°, 24.90°, respectively (Singh et al., 2017; Khoshnam and Salimijazi 2021). The planes at the (110), (101), and (002) support to confirm the crystalline structure of WO_3 is a wurtzite structure [Potti et al., 2012]

The XRD results showed as-prepared WO_3 mesosphere has a pure monoclinic crystal phase. Moreover, the crystallinity of the sample shows the positions of different atoms or molecules.

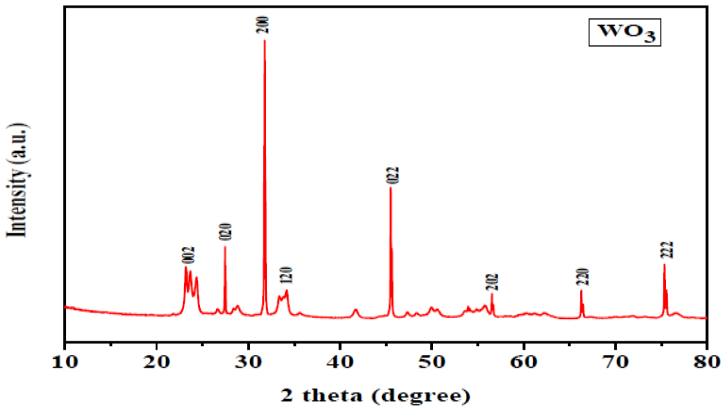

Figure 1: XRD analysis of different WO_3-based composite materials.

2. Surface morphological Analysis and Elemental dispersion X-ray analysis (EDX)

Scanning electron microscopy (SEM) analysis was used to confirm the surface morphology of the as-synthesized products. The WO_3 powder in Fig. 2 (a-c) shows the SEM images of WO_3 at different magnifications. It can be seen that the WO_3 contains a mixture of nanosphere about the range of 68 nm diameter with average breadths and lengths 34 nm and 132 nm, respectively. The inter-particle boundaries are almost invisible and confirmed the agglomerated nature of the particles from the images (Fig. 2a-c). Spherical particles of an average diameter of 78 nm display WO_3 nano sphere-like structures that display the hallow spherical type morphology. SEM image demonstrates that the prepared WO_3 is spherical in shape, scarcely dispersed, and finely distributed [Gu et al., 2005].

The elemental analyses of the as-synthesized WO_3 sample determined the chemical composition by using the EDS. Fig. 2d illustrates the EDS spectrum of some parts of the WO_3 sample and approves the creation of WO_3 during the photocatalysts as 49.9% W and 42.1% O atoms have existed in the 1: 1.1 ratio. From the results of the analysis, it is found that the relative content of W is slightly lower than the corresponding oxygen in WO_3 [Gu et al., 2002]. However, there is even a 1:1 ratio of W and oxygen signifying an increase in relative trend. While there was no noticeable number of other elements present and the diverse modification in the crystalline pattern and surface morphology supports the above results. Moreover, in spite of WO_3, there was the signal of carbon element at 1.5k intensity, this is the result of the carbon coating plate. Since the above results, the EDX analysis confirms about the as-prepared WO_3 nanospheres are exceedingly pure and lack a somewhat trace number of impurities.

3. FT-IR analysis

After calcinating at 400°C for 3h, the FT-IR spectra of as-synthesized materials are shown in Fig. 3. A strong absorption peak below the 400 cm^{-1} shows the presence of metal oxide nanoparticles which assistances in the inference of the WO_3. The primary intent of fabricating WO_3 with a high surface area was that it enabled IR spectroscopic studies of the surface groups and surface reactions. The diffuse reflectance (FTIR) spectra of the synthesized powder using a chelating agent and that recorded for commercial powder are shown in (fig. 3). The higher surface area enables the detection of bands due to surface OH and adsorbed water in the 3500cm^{-1} region. Specifically, the broad bands at 3450 and 3692 cm^{-1} are due to various O–H stretching modes and a sharp mode at 1636 cm^{-1} is the H_2O bending mode. In contrast, no bands were observed in the region 3433–1636 cm^{-1} in the FTIR spectrum of the commercial sample.

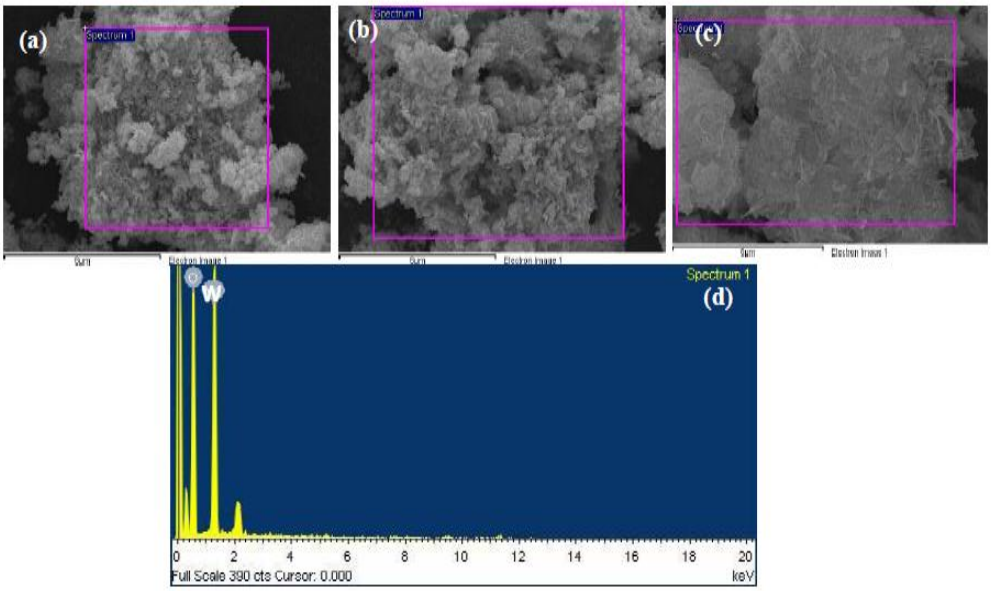

Figure 2: SEM analysis of WO_3 spherical catalyst at different magnification (a-c). EDAX analysis shows the elemental distribution of different WO_3 (d).

The region between 3500 - 1089 cm^{-1} contains bands due to both surface WOH and adsorbed water. By monitoring the change in intensity of the bending mode at 1636 cm^{-1}. It is possible to determine the degree of dehydration of the m-WO_3 with evacuation temperature. The dehydration curve indicates that about half of the total amount of adsorbed water is weakly adsorbed on the surface of WO_3 and easily removed with the evacuation at room temperature. In contrast, there is little change in the amount of water (15%) between separate WO_3 samples evacuated at 25℃ and 90^0C. As about 300% of the total adsorbed water remains strongly bound to the surface at 90^0 C. However, with the evacuation at increasing temperatures above 200^0C the amount of strongly bound water decreases and is completely removed only after evacuation at 400^0C [Wang et al., 2012].

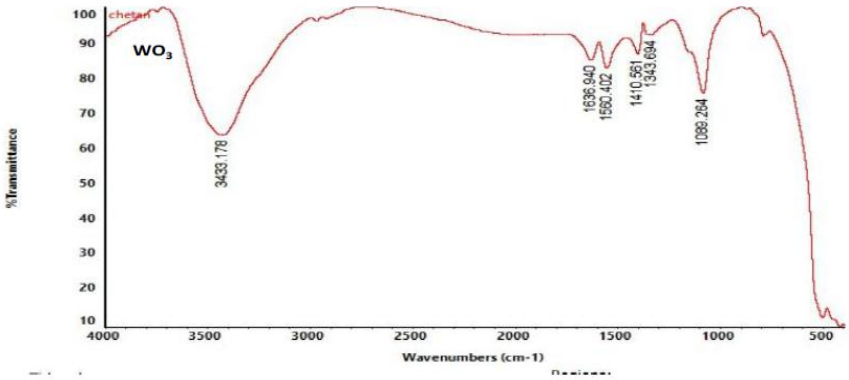

Figure 3: FTIR analysis of as-prepared WO_3 catalyst.

4. Effect of parameters

In most cases, industrial effluent has a pH range that spans a large range. As a result, measuring the pH of the test solution is critical in photocatalytic degradation.

4.1. Initial dye concentration

Rhodamine was employed as the chelator in the adsorption experiments because it is a good model for cationic dye removal from aqueous solutions. The influence of initial dye concentration on the dye degradation was studied using the rhodamine b dye concentration is 10-30 mgL^{-1} for keeping the WO_3 catalysts dose concentration is set at 1.0 g L^{-1} (Fig. 4). It is measured that the WO_3 sample degradation efficiency was first enhanced for dye concentrations increased from 10-30 mg L^{-1} and thereafter the removal was declined. The dye degradation efficiency decreased from 99% to 82% for WO_3, respectively when the concentration was increased from 10-30 mg L^{-1} (Fig. 4). It was used to compute adsorption capacity, with q equaling adsorptive capacity (mg g^{-1}), C equaling starting intensity, Cf equaling concentration at (final) equilibrium (mg L^{-1}), V

equaling volume of solutions (L), and S equaling mass of adsorption (g).

$$\text{Adsorptive capacity} = \frac{(\text{initial concentration} - \text{final concentration})\ \text{volume of the solution (L)}}{\text{Mass of the adsorbent (g)}}$$

The effect of an initial Rhodamine concentration in the range of 10-30 mgL^{-1}. As the initial Obtain the information concentrations grew, both rate constants began to fall. As the concentration grew, the number of intermediates increased as well, competing with the parent dye breakdown through reactive species. The goal is to introduce into the solution that is affected by the increasing dye content. The light intensity has a substantial impact on the reaction rate. As a result, the initial dye concentration might help enhance dye elimination competence. This might be observed that more dye molecules were adsorbed on the photocatalyst surface when the original dye concentration rises. Because numerous active sites are accessible and the dye molecules are occupied [Priyanka et al., 2014]. The photocatalysts' adsorption of OH^- and O_2 was minimized, resulting in less radical production. Additionally, photons were banned prior to the emergence of the photocatalysts' surface, resulting in a reduction in photon adsorption by the photocatalysts. The number of free radicals and the availability of the catalyst surface to absorption increase as the original dye concentration increases. Furthermore, at larger dye concentrations, repulsion between adjacent particles is strong enough that they remain separated and form a dispersion state. As a result, as the dye concentration rises, the dye removal diminishes. With less than 60 minutes of treatment time, the as-synthesized WO_3 catalyst achieves the highest results, degrading more than 95% of Rhodamine.

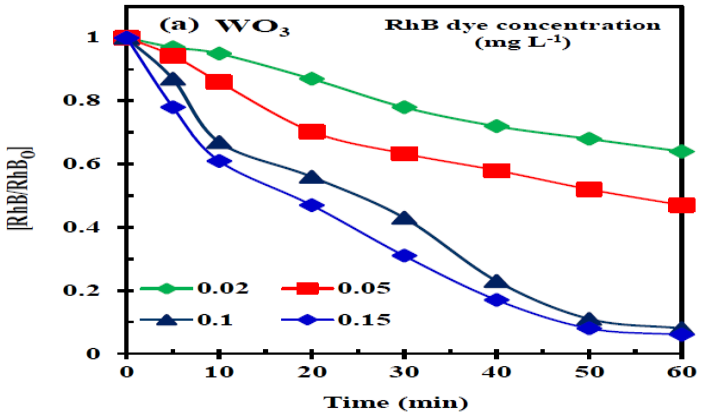

Figure 4: Effect of initial RhB concentration on the RhB degradation at the optimum treatment condition ([solution pH] = 7.0, catalyst dose=0.15 g L^{-1}, $[H_2O_2]_O$= 0.1 M and treatment volume is 250 mL at 25°C).

4.2. Effect of pH

Solution pH is a vital parameter in the treatment of dye effluents because it is an important element of the solution that has a substantial impact on the efficacy of photocatalysts. The photo-degradation efficiency of the photocatalysts generated was investigated at pH values ranging from 3 to 8. As shown in (Fig. 5). When the pH of such a dye concentration was elevated from 3 to 6.5, the study result much improved, then remained almost constant from 6.5 to 8. Over 88 percent of the removal was found at a pH of 8. pH is a complicated parameter since it is affected by various aspects, including the (i) surface's ionization state, (ii) The dye's composition, (iii) the thickness of the particle aggregation generated, and (iv) the degree of substrate adsorption on the active site [Wang et al., 2012].

An initial dye concentration of rhodamine b was fixed at about 10 mg L^{-1} in presence of UV- irradiation. The pH of the dye solution was fixed by the addition of hydrochloric acid (HCl), and sodium hydroxide (NaOH). It also clearly indicates that now the greatest results were achieved in a neutral solution, (pH=7). A zero-point charge shows catalysts on the surface outwardly positively charge in an acidic medium and negatively charged in a basic medium. The rhodamine b is an amphoteric dye. The Zero charged point of WO_3 is a huge range mentioned to the pH of 6.5 and has negatively charged pH greater than 6.25 orha positively charged at pH less than 6.5.

A pH less than zero improves the adsorption of rhodamine b dye molecules on photocatalyst surfaces, resulting in better RhB degradation of dyes in neutral and very less acidic conditions. These two techniques are suitable for dye degradation because rhodamine dye has a neutral charge attributed to the prevalence of negative charge including two groups: an amino group (NH_2) and one carboxylic group (COOH).

These results can be better appreciated by considering both the surface states of WO_3 and the ionization state of

the dye when the pH rises. The hydroxylated WO_3 surface may be protonated in an acidic environment and hydrolyzed in an alkaline environment, as shown in expression.

$WO_3 + H^+ \rightarrow WO_3H$ (in acidic medium)

$WO_3H + OH^- \rightarrow WO_3 + H_2O$ (in alkaline medium)

The maximum RhB removal with WO_3 at different pH of 3, 5, 7, and 8 were found to be around 48% to 96% for WO_3 (Fig.5).

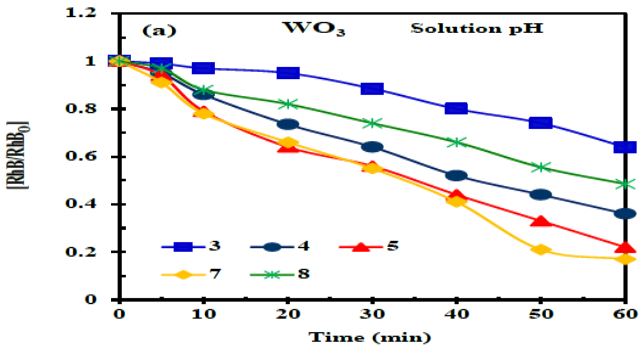

Figure 5: Effect of solution pH on the RhB dye degradation at the optimum treatment condition ([Catalyst dose] = 0.15 gL^{-1}, initial pollutant concentration=10 mgL^{-1}, $[H_2O_2]_o$= 0.1 M and treatment volume is 250 mL at 25°C).

4.3. Effect of catalysts

Even though WO_3 is an enticing photocatalyst for destroying utterly pointless and harmful organic molecules in water, combining it with a variety of other materials to strap the personal components' strong points, as well as the symbiotic benefits of the composite, as well as the synergistic advantages of the reinforcement, could result in a visible-light-sensitive and high-performing catalyst. There is another important factor is the effect of catalysts' dose on dye degradation was studied during the treatments. As the catalyst dose increases, the dye degradation efficiency successively increases WO_3. The impact of catalyst doses of 0.02, 0.05, 0.1, and 0.15 gL^{-1} in 250 mL of dye fixed concentration of 10 mgL^{-1} and a neutral pH of rhodamine B dye was investigated (Fig. 6). Although WO_3 alone could eliminate the dye, the elimination rate was low (as seen in Fig. 6), but increasing the WO_3 dosage from 0.02-1.5 gL^{-1} substantially increased the removal of dye. As shown in (Fig. 6),when WO_3 doses were 0.02 gL^{-1}, 28 to 42 percent RhB was degraded after 60 minutes, whereas more than 90 percent RhB was eliminated after 70 minutes when WO_3 dosages were 1.5 gL^{-1}, albeit there was a slight change in elimination when the catalyst dose was increased. This improvement occurred because higher WO_3 doses may provide more active sites for H_2O_2 activation [Lou et al., 2013].

In light of the foregoing, WO_3 was considered as the most suitable catalyst, with a catalyst dose of 1.5 gL^{-1} being chosen as the best amount in this investigation. This is due to the higher catalyst concentration, which restricts optimum light absorption and, as a result, reduces dye photodegradation. As a consequence, 1.5 gL^{-1} was chosen as the best catalyst dose for future photocatalytic degradation testing. In a study of four as-prepared catalysts, WO_3 was shown to have the best photocatalytic activity for rhodamine B degradation of dyes.

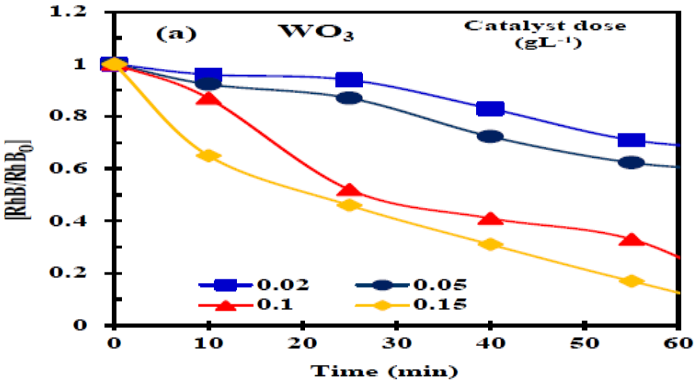

Figure 6: Effect of catalyst dose on the RhB dye degradation at the optimum treatment condition [solution pH] = 6.0, initial pollutant concentration=10 mgL^{-1}, $[H_2O_2]_O$= 0.1 M and treatment volume is 250 mL at 25°C).

4.4. XRD pattern of WO_3 after RhB removal

Fig. 7 shows the XRD pattern of recovered catalysts that are collected after the last cycle of the experimental test. XRD pattern showed, no impurity peaks of reused catalyst that show no photo-corrosion and leaching of the catalyst through the pollutant reduction. All in all, the crystallinity of the post-degradation catalyst is still almost reserved and shows the excellent stability and robustness of the catalyst under the reaction condition.

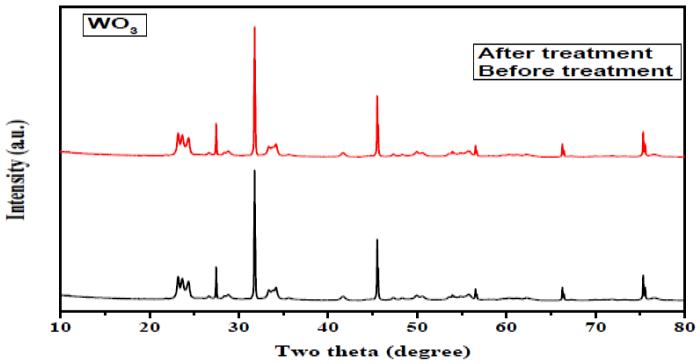

Figure 7: XRD analysis before and after treatment.

4.5. Reusability of WO_3 mesosphere

From the economic and potential applications point of view, the regeneration and reusability of photocatalyst materials are significant aspects to be described. Conventional separation methods i.e., centrifugation and filtration are used to separate the catalyst from the treatment solution [Singh et al., 2013]. Consequently, RhB degradation experiments were conducted to evaluate the reusability of the nanocomposite. Between each experiment, the samples were collected by centrifugation and filtration and then washed with ethanol and deionized water for some time and dried at 90^{o}C for 80 min. Fig. 8 shows that photodegradation effectiveness is somewhat significantly reduced. This decrease in the percentage of removal efficiency perhaps was ascribed to little loss of WO_3 mesosphere from the support surface through the washing procedure. The additional possible purpose is the accumulation of intermediate by-products formed by the organic pollutant degradation on the active surface of the photocatalyst, which in go decreases the photocatalytic activity. Consequently, the mesosphere photocatalyst was recovered after five cycles. The recovered catalyst was calcined at 600^{o}C for 3 hours and then reused. The attained result proves that thermal recurrence leads to substantial regeneration of photocatalytic activity. Therefore, it can be stated that thermally treatment is an essential process for the used catalyst to the regeneration of its activity.

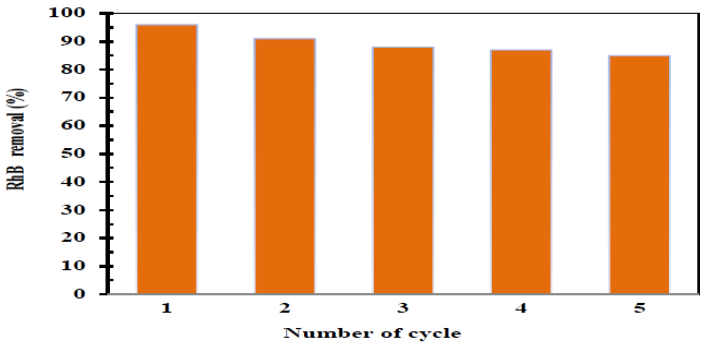

Figure 8: Reusability test analysis of WO_3 catalyst in RhB dye degradation. Experimental conditions: [catalyst dose] = 1.5 g L^{-1}, [RhB] = 10 mg L^{-1}, pH = 7.

5. CONCLUSION

Precipitation in the presence of citric acid at various temperatures resulted in highly crystalline WO_3 nanoparticles with a monoclinic structure. To assess the morphology, surface roughness, and particle size, XRD, EDX, and FTIR studies were performed. Morphology of WO_3 after examination with various methods was confirmed to be rectangular and oval shape particles. The potential of WO_3 nanomaterial to catalyze photodegradation of RhB dye in an aqueous solution was determined at various pH. Throughout the experiments with Vis and UV radiation, it was possible to conclude that the degradation of RhB by WO_3 seems to occur predominantly through the photosensitization of the organic dye by the action of visible-light irradiation. Finally, the formation and participation of •OH radicals in the degradation of organic dyes when WO_3 is used as a photocatalyst was confirmed.

REFERENCES

1. Kiwaan, H. A., Atwee, T. M., Azab, E. A., & El-bindary, A. A. Photocatalytic degradation of organic dyes in the presence of nanostructured titanium dioxide. Journal of Molecular Structure, 2020; 1200: 127115. https://doi.org/10.1016/j.molstruc.2019.127115
2. Karthikeyan, C., Arunachalam, P., Ramachandran, K., Al-mayouf, A. M., & Karuppuchamy, S. Reproduced from reference [34] with permission from Elsevier Graphical Abstract C. Karthikeyan et al. Journal of Alloys and Compounds, 2020; 154281.
3. Kishor, R., Purchase, D., Dattatraya, G., Ganesh, R., Fernando, L., Ferreira, R., Bilal, M., Chandra, R., & Naresh, R. Journal of Environmental Chemical Engineering Ecotoxicological and health concerns of persistent coloring pollutants of textile industry wastewater and treatment approaches for environmental safety. Journal of Environmental Chemical Engineering, 2021; 9(2): 105012. https://doi.org/10.1016/j.jece.2020.105012
4. Konstantinou, I. K., & Albanis, T. A. TiO_2-assisted photocatalytic degradation of azo dyes in aqueous solution: Kinetic and mechanistic investigations: A review. Applied Catalysis B: Environmental, 2004; 49(1): 1-14. https://doi.org/10.1016/j.apcatb.2003.11.010
5. Drumond Chequer, F. M., de Oliveira, G. A. R., Anastacio Ferraz, E. R., Carvalho, J., Boldrin Zanoni, M. V., & de Oliveir, D. P. Textile Dyes: Dyeing Process and Environmental Impact. Eco-Friendly Textile Dyeing and Finishing, 2013. https://doi.org/10.5772/53659
6. Hassani, A., Alidokht, L., Khataee, A. R., & Karaca, S. Optimization of comparative removal of two structurally different basic dyes using coal as low-cost and available adsorbent. Journal of the Taiwan Institute of Chemical Engineers, 2014; 45(4): 1597-1607. https://doi.org/10.1016/j.jtice.2013.10.014
7. Shindhal, T., Rakhoilya, P., Varjani, S., Pandey, A., Ngo, H. H., Guo, W., Ng, H. Y., & Taherzadeh, M. J. A critical review on advances in the practices and perspectives for the treatment of dye industry wastewater. *Bioengineered*, 2021; 12(1): 70-87. https://doi.org/10.1080/21655979.2020.1863034
8. Saravanan, R., Gupta, V. K., Mosquera, E., Gracia, F., Narayanan, V., & Stephen, A. Visible light induced degradation of methyl orange using β-$Ag_{0.333}V_2O_5$ nanorod catalysts by facile thermal decomposition method. *Journal of Saudi Chemical Society*, 2015; 19(5): 521-527. https://doi.org/10.1016/j.jscs.2015.06.001
9. Ahmed, N. S. E. The use of sodium edate in the dyeing of cotton with reactive dyes. *Dyes and Pigments*, 2005; *65*(3): 221-225. https://doi.org/10.1016/j.dyepig.2004.07.014
10. Hai, F. I., Yamamoto, K., & Fukushi, K. Hybrid treatment systems for dye wastewater. *Critical Reviews in Environmental Science and Technology*, 2007; *37*(4): 315-377. https://doi.org/10.1080/10643380601174723
11. Bhatia, D., Sharma, N. R., Singh, J., & Kanwar, R. S. Biological methods for textile dye removal from wastewater: A review. *Critical Reviews in Environmental Science and Technology*, 2017; *47*(19): 1836-1876. https://doi.org/10.1080/10643389.2017.1393263
12. Martinez-Huitle, C. A., & Brillas, E. Decontamination of wastewaters containing synthetic organic dyes by electrochemical methods: A general review. *Applied Catalysis B: Environmental*, 2009; 87(3-4): 105-145. https://doi.org/10.1016/j.apcatb.2008.09.017
13. Forgacs, E., Cserháti, T., & Oros, G. Removal of synthetic dyes from wastewaters: A review. *Environmental International*, 2004; *30*(7): 953-971. https://doi.org/10.1016/j.envint.2004.02.001
14. Robinson T, Mcmullan G, Marchant R, Nigam P, Remediation of dyes in textile euent: a critical review on current treatment technologies with a proposed alternative, Bioresource Technology, 2001; 77: 247±255.
15. Samsami, S., Mohamadi, M., Sarrafzadeh, M. H., Rene, E. R., & Firoozbahr, M. Recent advances in the treatment of dye containing wastewater from textile industries: Overview and perspectives. *Process Safety and Environmental Protection*, 2020; *143*: 138-163. https://doi.org/10.1016/j.psep.2020.05.034
16. Akpomie, K. G., & Conradie, J. Advances in application of cotton-based adsorbents for heavy metals trapping, surface modifications and future perspectives. *Ecotoxicology and Environmental Safety*, *2020; 201:* 110825. https://doi.org/10.1016/j.ecoenv.2020.110825
17. Khataee, A. R., Pons, M. N., & Zahraa, O. Photocatalytic degradation of three azo dyes using immobilized TiO_2 nanoparticles on glass plates activated by UV light irradiation: Influence of dye molecular structure. *Journal of Hazardous Materials, 2009; 168*(1)*:* 451-457. https://doi.org/10.1016/j.jhazmat.2009.02.052
18. Al-Mutairi, N. Z. Coagulant toxicity and effectiveness in a slaughterhouse wastewater treatment plant. *Ecotoxicology and Environmental Safety*, *2006;* 65(1): 74-83. https://doi.org/10.1016/j.ecoenv.2005.05.013
19. Zarei Mahmudabadi T., Ebrahimi, A. A., Eslami, H., Mokhtari, M., Salmani, M. H., Ghaneian, M. T., Mohamadzadeh, M., & Pakdaman, M. Optimization and economic evaluation of modified coagulation-flocculation process for enhanced treatment of ceramic-tile industry wastewater. *AMB Express*, 2018; *8*(1). https://doi.org/10.1186/s13568-018-0702-4
20. Rahmani, A. R., Mousavi-Tashar, A., Masoumi, Z., & Azarian, G. (2019). Integrated advanced oxidation process, sono-fenton treatment, for mineralization and volume reduction of activated sludge.

Ecotoxicology and Environmental Safety, 2019; 168(2018): 120-126. https://doi.org/10.1016/j.ecoenv.2018.10.069

21. Li, H., Xue, S., Cao, Y., Yue, X., Zhang, A., & Chen, C. Photocatalytic reduction of Cr(VI) by WO_3@PVP with elevated conduction band level and improved charge carrier separation property. *Environmental Science and Ecotechnology, 2020;* 3(Vi): 100034. https://doi.org/10.1016/j.ese.2020.100034
22. Siwińska-Stefańska, K., Kubiak, A., Piasecki, A., Goscianska, J., Nowaczyk, G., Jurga, S., & Jesionowski, T. TiO_2-ZnO binary oxide system: Comprehensive characterization and tests of photocatalytic activity. *Materials, 2018; 11(5):* 1-19. https://doi.org/10.3390/ma11050841
23. Hassanshahi, N., & Karimi-Jashni, A. Comparison of photo-fenton, O_3/H_2O_2 /UV and photocatalytic processes for the treatment of gray water. *Ecotoxicology and Environmental Safety, 2018; 161:* 683-690. https://doi.org/10.1016/j.ecoenv.2018.06.039
24. Andreozzi, R., Caprio, V., Insola, A., & Marotta, R. Advanced oxidation processes (AOP) for water purification and recovery. *Catalysis Today, 1999; 53*(1): 51-59. https://doi.org/10.1016/S0920-5861(99)00102-9
25. Oturan, M. A., & Aaron, J. J. Advanced oxidation processes in water/wastewater treatment: Principles and applications. A review. *Critical Reviews in Environmental Science and Technology, 2014; 44*(23): 2577-2641. https://doi.org/10.1080/10643389.2013.829765
26. Nazri, M. K. H. M., & Sapawe, N. A short review on photocatalytic toward dye degradation. *Materials Today: Proceedings, 2020; 31:* A42-A47. https://doi.org/10.1016/j.matpr.2020.10.967
27. Mills A, Hunte S.L, An Overview of semiconductor photocatalysis, Journal of Photochemistry and Photobiology A: Chemistry, 1997; 108: 1-35.
28. Beydoun, D., Amal, R., Low, G., & McEvoy, S. Role of nanoparticles in photocatalysis. *Journal of Nanoparticle Research, 1999; 1*(4): 439-458. https://doi.org/10.1023/A:1010044830871
29. Gupta, S. M., & Tripathi, M. A review of TiO_2 Nanoparticles. *Chienese Science Bulletin, 2011;* 56(16): 1639-1657. https://doi.org/10.1007/s11434-011-4476-1
30. Mokif, L. A. *Removal Methods of Synthetic Dyes From Industrial Wastewater: A Review, 2019;* 5(1): 23-40.
31. Mondal, S. *Methods of Dye Removal From Dye House Effluent, 2008;* 25(3). https://doi.org/10.1089/ees.2007.0049
32. Khan, I., Saeed, K., Ali, N., Khan, I., Zhang, B., & Sadiq, M. *Journal of Environmental Chemical Engineering Heterogeneous photodegradation of industrial dyes: An insight to different mechanisms and rate affecting parameters, 2020;* 8(June). https://doi.org/10.1016/j.jece.2020.104364
33. Melinte V, Stroea L, Chibac-Scutaru A. L, Polymer Nanocomposites for photocatalytic applications, 2019. doi:10.3390/catal9120986.
34. Kumar, A., & Pandey, G. *A review on the factors affecting the photocatalytic degradation of hazardous materials. November, 2018.*
35. Gnanaprakasam, A., Sivakumar, V. M., & Thirumarimurugan, M. *Influencing Parameters in the Photocatalytic Degradation of Organic Effluent via Nanometal Oxide Catalyst: A Review, 2015.*
36. Palai, A., Ranjan, N., & Sahu, D. Novel ZnO blended SnO_2 nanocatalysts exhibiting superior degradation of hazardous pollutants and enhanced visible photoemission properties. *Journal of Molecular Structure, 2021; 1244:* 131245. https://doi.org/10.1016/j.molstruc.2021.131245
37. Sun, C., Yang, J., Xu, M., Cui, Y., Ren, W., Zhang, J., Zhao, H., & Liang B. Recent intensification strategies of SnO_2 - based photocatalysis : A review. *Chemical Engineering Journal, 2022; 427*(2021): 131564. https://doi.org/10.1016/j.cej.2021.131564
38. Sood, S., Kumar, S., Umar, P. A., Kaur, A., Mehta, S. K., Sushil, P., & Kansal, K. SC. *Journal of Alloys and Compounds, 2015.* https://doi.org/10.1016/j.jallcom.2015.07.164
39. Deshmukh, K. K., Hase, G. J., Gaje, T. R., & Narendra, D. *Titanium Oxide Nanoparticles and Degradation of Dye By Nanoparticles, 2018; 13*(1): 23-30.
40. Danwittayakul, S., Jaisai, M., & Dutta, J. Applied Catalysis B: Environmental Efficient solar photocatalytic degradation of textile wastewater using ZnO / ZTO composites. "*Applied Catalysis B, Environmental,", 2015; 163:* 1-8. https://doi.org/10.1016/j.apcatb.2014.07.042
41. Pare, B., Jonnalagadda, S. B., Tomar, H., Singh, P., & Bhagwat, V. W. ZnO assisted photocatalytic degradation of acridine orange in aqueous solution using visible irradiation. *Desalination, 2008; 232*(1-3): 80-90. https://doi.org/10.1016/j.desal.2008.01.007
42. Muthirulan, P., Meenakshisundararam, M., & Kannan, N. Beneficial role of ZnO photocatalyst supported with porous activated carbon for the mineralization of alizarin cyanin green dye in aqueous solution. *Journal of Advanced Research, 2013; 4*(6): 479-484. https://doi.org/10.1016/j.jare.2012.08.005
43. Desai, K. R., Pathan, A. A., & Bhasin, C. P. Synthesis, Characterization of Cadmium Sulphide nanoparticles and its Application as Photocatalytic Degradation of Congored. *International Journal of Nanomaterials and Chemistry, 2017; 3*(2): 39-43. https://doi.org/10.18576/ijnc/030204
44. Ullah, H., Viglašová, E., & Galamboš, M. Visible light-driven photocatalytic rhodamine B degradation using CdS nanorods. *Processes, 2021; 9*(2): 1-11. https://doi.org/10.3390/pr9020263
45. Venkatesh, N., Sabarish, K., Murugadoss, G., & Thangamuthu, R. *Visible light- driven*

phtotocatalytic dye degradation under natural sunlight using Sn-doped CdS nanoparticles, 2020.

46. Sadeghzadeh-Attar A, Efficient photocatalytic degradation of methylene blue dye by SnO_2 nanotubes synthesized at different calcinations temperatures, 2018. https://doi.org/10.1016/j.ijleo.2021.167152
47. Najjar, M., Ali, H., Masoudi, A., Sabouri, Z., Mostafapour, A., Khatami, M., & Darroudi, M. Optik Green chemical approach for the synthesis of SnO_2 nanoparticles and its application in photocatalytic degradation of Eriochrome Black T dye. *Optik, 2021; 242:* 167152. https://doi.org/10.1016/j.ijleo.2021.167152
48. Gnana, S. E., Rani, D., Kumar, A. G., Rajaram, R., Silambarasan, T. S., Lydia, S., & Chen, Y. ur 1 P re. *Science of the Total Environment, 2020;* 137805. https://doi.org/10.1016/j.scitotenv.2020.137805
49. Bamwenda, G. R., & Arakawa, H. Visible light induced photocatalytic activity of tungsten trioxide powders. *Applied Catalysis A: General, 2001; 210*(1-2): 181-191. https://doi.org/10.1016/S0926-860X(00)00796-1
50. Sayama, K., Hayashi, H., Arai, T., Yanagida, M., Gunji, T., & Sugihara, H. Highly active WO_3 semiconductor photocatalyst prepared from amorphous peroxo- tungstic acid for the degradation of various organic compounds. *Applied Catalysis B: Environmental, 2010; 94*(1-2): 150-157. http://doi.org/10.1016/j.apcatb.2009.11.003
51. Calero¸ S. J., Ortiz, P., Oñate, A. F., & Cortés, M. T. Effect of proton intercalation on photo-actvity of WO_3 anodes for water splitting. *International Journal of Hydrogen Energy, 2016; 41*(9): 4922-4930. https://doi.org/10.1016/j.ijhydene.2015.12.155
52. S. Wang, H. Yang, Z. Yi, X. Wang, Enhanced photocatalytic performance by hybridization of Bi_2WO_6 nanoparticles with honeycomb- like porous carbon skeleton, Journal of Environmental Management, 2019; 248: 109341
53. C. Zhang, G. Chen, C. Li, J. Sun, C. Lv, S. Fan, W. Xing, In situ fabrication of Bi_2WO_6/MoS_2/RGO heterojunction with nanosized interfacial contact via confined space effect towards enhanced photocatalytic properties, ACS Sustainable Chem. Eng, 2016; 4, 11: 5936-5942.
54. X. Ren, K. Wu, Z. Qin, X. Zhao, H. Yang, The construction of type II heterojunction of Bi_2WO_6/BiOBr photocatalyst with improved photocatalytic performance, Journal of Alloys and Compounds, 2019; 788: 102-109.
55. J. Li, Y. Zhao, M. Xia, H. An, H. Bai, J. Wei, B. Yang, G. Yang, Highly efficient charge transfer at 2D/2D layered P-$La_2Ti_2O_7/Bi_2WO_6$ contact heterojunctions for upgraded visible-light driven photocatalysis, Applied Catalysis B: Environmental, 2020; 261: 118244.
56. S. Jonjana, A. Phuruangrat, S. Thongtem, T. Thongtem, Synthesis, characterization and photocatalysis of heterostructure AgBr/Bi_2WO_6 nanocomposites, Materials Letters, https://doi.org/10.1016/j.matlet.2018.01.005
57. X. Qian, D. Yue, Z. Tian, M. Ren, Y. Zhu, M. Kan, T. Zhang, Y. Zhao, Carbon quantum dots decorated Bi_2WO_6 nanocomposite with enhanced photocatalytic oxidation activity for VOCs, Applied Catalysis B: Environmental, http://dx.doi.org/doi:10.1016/j.apcatb.2016.04.009
58. B. Li, C. Lai, G. Zeng, L. Qin, H. Yi, D. Huang, C. Zhou, X. Liu, M. Cheng, P. Xu, C. Zhang, F. Huang, S. Liu, Facile Hydrothermal Synthesis of Z-scheme $Bi_2Fe_4O_9/Bi_2WO_6$ Heterojunction photocatalyst with Enhanced Visible-Lig
59. I. F. Ertis, I. Boz. Synthesis and Characterization of Metal- Doped (Ni, Co, Ce, Sb) CdS Catalysts and Their Use in Methylene Blue Degradation Under Visible Light Irradiation. Journal of *Modern Research in Catalysi.* doi:10.4236/mrc.2017.61001
60. S. R. Chandran, A. Sivasamy, B. D Kumar. Nitrogen doped nanocrystalline semiconductor metal oxide: An efficient UV active photocatalyst for the oxidation of an organic dye using slurry photoreactor Journal of Ecotoxicology and Environmental Safety doi:10.1016/j.ecoenv.2016.01.022
61. Y. Zhang, G. Zhao, L. Gan, H. Lian, M. Pan. S-doped carbon nanosheets supported ZnO with enhanced visible –light photocatalytic performance for pollutants degradation. Journal of Cleaner Production, 2021; 319: 128803. S. Bera, D. Won, S. B. Rawal, H. J. Kang, W. I. Lee. Design of visible – light photocatalysts by coupling of inorganic semiconductors. Journal of Catalysis Today
62. T. M. S. Dawoud, V. Pavitra, P. Ahmad, A. Syed, G. Nagaraju. Photocatalytic degradation of an organic dye using Ag doped ZrO_2 nanoparticles: Milk powder facilitated eco-friendly synthesis. Journal of King Saud University – Science doi.org/10.1016/j.jksus.2020.01.040.
63. S. G. Shelar, V. K. Mahajan, S. P. Patil, G. H. Sonawane Effect of doping parameters on photocatalytic degradation of methylene blue using Ag doped ZnO nanocatalyst Journal of SN Applied Sciences doi:10.1007/s42452-020-2634-2.
64. A. Khanna, V. K. Shetty. Solar light induced photocatalytic degradation of Reactive Blue 220 (RB-220) dye with highly efficient Ag@TiO_2 core-shell nanoparticles: A comparison with UV photocatalysis. Journal of Solar Energy, 2013; 99: 6776.
65. A. Nibret, O. P. Yadav, I. Diaz, A. M. Taddesse, Cr-N co-doped ZnO Nanoparticles: synthesis, characterization and photocatalytic activity for degradation of thymol blue. Journal of Bulletin of the Chemical Society Ethiop, 2015; 29(2): 247-258.
66. S. Singh, V. C. Srivastava, I. D. Mall, Electrochemical treatment of dye bearing effluent with different anode-cathode combinations: Mechanistic study and sludge analysis, Ind. Eng. Chem. Res, 2014; 53: 10743-10754.

67. P. R. Potti, V. C. Srivastava, Comparative studies on structural, optical, and textural properties of combustion derived ZnO prepared using various fuels and their photocatalytic activity, Ind. Eng. Chem. Res, 2012; 51: 7948-7956.
68. Z. Gu, Y. Ma, W. Yang, G. Zhang, J. Yao, Self-assembly of highly oriented one-dimensional h-WO_3 nanostructures, Chem. Commun, 2005; 41: 3597-3599.
69. J. Su, X. Feng, J. D. Sloppy, L. Guo, C. A. Grimes, Vertically aligned WO_3 nanowire arrays grown directly on transparent conducting oxide coated glass: synthesis and photo electrochemical properties, Nano Lett, 2011; 11: 203-208.
70. W. Smith, A. Wolcott, R. C. F. morris, J. Z. Zhang, Y. P. Zhao, Quasi-core-shell TiO_2/WO_3 and TiO_2/WO_3 nanorod arrays fabricated by glancing angle deposition for solar water splitting, J. Mater. Chem, 2011; 21: 10792-10800.
71. G. Gu, B. Zheng, W. Han, S. Roth, J. Liu, Tungsten Oxide nano wires on tungusten substrates, Nano Lett, 2002; 2: 849-851.
72. G. Wang, Y. Ling, Y. Li, Oxygen-deficient metal oxide nanostructures for photoelectrochemical water oxidation and other applications, Nanoscale, 2012; 4: 6682-6691.
73. Priyanka, V. Subbaramaiah, V.C. Srivastava, I. D. Mall, Catalytic oxidation of nitrobenzene by copper loaded activated carbon. Sep. Purif. Technol, 2014; 125: 284-90.
74. X. Lou, H. Zeng, An inorganic route for controlled synthesis of $W_{18}O_{49}$ nanorods and nanofibers in solution, Inorg. Chem, 2003; 42: 6169-6171.
75. S. Singh, V. C. Srivastava, I. D. Mall, Mechanism of dye degradation during electrochemical treatment, J. Phy. Chem. C, 2013; 117: 15229-15240.